Air quality observations onboard commercial and targeted Zeppelin flights in Germany - a platform for high-resolution trace-gas and aerosol measurements within the planetary boundary layer

Ralf Tillmann[1], Georgios I. Gkatzelis[1], Franz Rohrer[1], Benjamin Winter[1], Christian Wesolek[1], Tobias Schuldt[1], Anne C. Lange[1], Philipp Franke[1], Elmar Friese[1], Michael Decker[1], Robert Wegener[1], Morten Hundt[2], Oleg Aseev[2], Astrid Kiendler-Scharr[1]

[1] Institute of Energy and Climate Research, IEK-8: Troposphere, Forschungszentrum Jülich GmbH, Jülich, Germany

[2] MIRO Analytical AG, Wallisellen, 8304, Switzerland

Correspondence to: Ralf Tillmann (r.tillmann@fz-juelich.de)

Abstract.

A Zeppelin airship was used as a platform for in-situ measurements of greenhouse gases and short-lived air pollutants within the planetary boundary layer (PBL) in Germany. A novel quantum cascade laser-based multi-compound gas analyzer (MIRO Analytical AG) was deployed to simultaneously measure in-situ concentrations of greenhouse gases (CO_2, N_2O, H_2O, and CH_4) and air pollutants (CO, NO, NO_2, O_3, SO_2, and NH_3) with high precision at a measurement rate of 1 Hz. These measurements were complemented by electrochemical sensors for NO, NO_2, O_x (NO_2+O_3), and CO, an optical particle counter, temperature, humidity, altitude, and position monitoring. Instruments were operated remotely without the need for on-site interactions. Three two-week campaigns were conducted in 2020 comprising commercial passenger as well as targeted flights over multiple German cities including Cologne, Mönchengladbach, Düsseldorf, Aachen, Frankfurt, but also over industrial areas and highways.

Vertical profiles of trace gases were obtained during the airship landing and take-off. Diurnal variability of the Zeppelin vertical profiles was compared to measurements from ground-based monitoring stations with a focus on nitrogen oxides and ozone. We find that their variability can be explained by the increasing nocturnal boundary layer height from early morning towards midday, an increase in emissions during rush hour traffic, and the rapid photochemical activity midday. Higher altitude (250–450 m) NO_x to CO ratios are further compared to the 2015 EDGAR emission inventory to find that pollutant concentrations are influenced by transportation and residential emissions as well as manufacturing industries and construction activity. Finally, we report NO_x and CO concentrations from one plume transect originating from a coal power plant and compare it to the EURAD-IM model to find agreement within 15%. However, due to the increased contribution of solar and wind energy and/or the impact of lockdown measures the power plant was operated at max. 50% capacity; therefore, possible overestimation of emissions by the model cannot be excluded.

1 Introduction

Favorable meteorological conditions can trigger severe pollution episodes in which anthropogenic emissions of pollutant concentrations accumulate and drastically exceed the ~~world~~ World ~~health~~ Health ~~organization~~ Organization (WHO) guideline values. Meteorologically induced air pollution is consistently observed globally in Asia (He et al., 2017; Li et al., 2019; Cai et al., 2017; Zhao et al., 2019), America (Jury, 2020; Zhao et al., 2011; Lin and McElroy, 2010), and Europe (Dupont et al., 2016; Pernigotti et al., 2012) even during periods when certain anthropogenic emission sectors are diminished (Gkatzelis et al., 2021a). With air quality being the number one environmental health risk globally (WHO, 2021; Lelieveld et al., 2015), there is an increasing need to monitor pollutant concentrations in time and amplitude in order to identify the driving factors for degraded air quality. An essential first step towards this goal is to accurately determine the effect of local meteorological parameters such as surface relative humidity, wind speed, turbulence, and planetary boundary layer (PBL) depth development on pollutant concentrations. Up to date, various studies highlight the need for accurate PBL depth data as they pose the most uncertain parameter for efficient air quality forecasts (e.g., Dupont et al., 2016; Lin and McElroy, 2010; Silcox et al., 2012; Horel et al., 2016). Vertical mixing of air tracers within the PBL can influence their tropospheric distributions with a turbulent mixed layer leading to a more uniform vertical distribution and a stable boundary layer resulting in greater vertical gradients.

Numerous European ground-based networks e.g., the European Environment Agency, EEA, together with the European Monitoring and Evaluation Programme, EMEP (http://ebas.nilu.no), or from infrastructures such as the Aerosols, Clouds and Trace gases Research Infrastructure (ACTRIS; https://www.actris.eu/) provide data for criteria pollutant concentrations worldwide; however, there is still a lack of information along the vertical. Satellite retrievals allow global coverage of pollutant concentrations but only obtain the nadir total column with limited information on the vertical distribution of pollutant concentrations (e.g., Veefkind et al., 2012). On the other hand, aircraft campaigns provide pollutant concentrations at various altitudes (e.g., Molina et al., 2010; Ryerson et al., 2013; Benedict et al., 2019); however, obtaining vertical profiles is challenging and the data availability is limited due to high rental aircraft costs. A way to overcome such a limitation has been to deploy instrumentation in commercial airliners as has been done in the last decades by the In-service Aircraft for a Global Observing System (IAGOS; https://www.iagos.org; Marenco et al., 1998; Petzold et al., 2015). Such measurements provide regular data on the PBL dynamics but are limited to areas in proximity to airport locations during the aircraft's landing and take-off (Boschetti et al., 2015). Commercial airborne measurements have also been extended to routine helicopter flights to monitor vertical profiles for pollutant concentrations in Utah, USA (Crosman et al., 2017). Balloon-borne (e.g., Ouchi et al., 2019) and small unmanned aerial vehicles i.e., drones (Villa et al., 2016) are also frequently used for vertical profile measurements; however, they cover a limited number of pollutants due to weight restrictions. Finally, ground-based LIDAR measurements can provide a diagnosis on the PBL height and vertical concentration profiles but are often limited to only one pollutant (e.g., Dang et al., 2019).

A Zeppelin is an ideal airborne platform to capture the vertical distribution of pollutant concentrations and gain insights into their origin and emission sources (Lampilahti et al., 2021; Li et al., 2014; Nieminen et al., 2015). It offers enough room to deploy equipment and flies precisely and slowly at desired heights. Such airborne

measurements provide unique opportunities to compare to modeling efforts and evaluate and update air quality forecasts and emission inventories for single point sources.

Here, we present commercial and targeted Zeppelin flights in Germany using state-of-the-art instrumentation to investigate the vertical, spatial, and temporal distribution of pollutant concentrations including nitrogen oxides (NO, NO_2, and NO_x), ozone (O_3), carbon monoxide (CO), carbon dioxide (CO_2), and others. We compare these results to observations from ground-based monitoring stations and emission inventory estimates. Finally, we report emissions from a coal power plant and compare our measurements to the EURAD-IM model hindcast (Elbern et al., 2007).

2 Methods

2.1 Zeppelin platform

The airborne platform used in this study was the Zeppelin New Technology (NT) developed by Zeppelin Luftschifftechnik GmbH & CO. KG (ZLT) in Friedrichshafen, Germany, in 1997. Zeppelin NT is an economical airship with a length of 75 m, a diameter of about 14 m, and a maximum payload of around 1.8 tons. It offers a unique combination of capabilities not available in other airborne platforms including a high scientific payload, high maneuverability in all directions due to a vectored thrust propulsion system, flight speeds from 0–115 km/h, a horizontal reach of up to more than 600 km, operating altitude of 20–1500 m, and a maximum flight endurance of 15 h.

Figure 1A shows the Zeppelin flights over Germany and Figure 1B the vertical and diurnal distribution of these flights. Detailed information on the take-off and landing times, airport locations, and flight paths are provided in Table 1. In this study, 14 days of commercial flights, 4 days of targeted flights, and 6 days of transect flights with overall 172 take-offs and landings were performed and analyzed. The Zeppelin flew over various cities, including Cologne, Mönchengladbach, Düsseldorf, Aachen, Jülich, Frankfurt, but also over industrial areas, and highways. The majority of the measurements ranged from 200 to 450 m in altitude. Measurements below 200 m were predominantly during the Zeppelin landing and take-off periods and higher altitude measurements above 400 m were during transect and targeted flights. Flights were distributed in summer 2020 to 9, 7, and 10 flight days in May, June, and September, respectively, ranging from 3–10 flight hours per day. Four airports were chosen to refuel the Zeppelin, namely, Friedrichshafen, Bonn-Hangelar, Mönchengladbach, and the Bad Homburg airfield.

Zeppelin NT has been previously used as an airborne platform fully equipped with instrumentation to conduct atmospheric research during the PEGASOS project (Li et al., 2014; Nieminen et al., 2015). Here, measurements were predominantly performed during commercial passenger flights providing low costs but limited space to deploy instrumentation. Two main instrument setups were fitted in the cabin of the Zeppelin: the MIRO instrument and the hatch box with diverse low-cost sensors as discussed in the following sections.

Table 1: Zeppelin flight details.

Date	Local start time	Local end time	Airport Code	Flight Details
29.04.2020	8:17:00	15:00:00	FDH– BNJ	Friedrichshafen - Bonn/Hangelar
05.05.2020	9:43:00	16:22:00	BNJ	Köln & Mönchenlagdbach
06.05.2020	7:14:00	14:30:00	BNJ	Weisweiler
07.05.2020	8:30:00	15:30:00	BNJ	Mönchengladbach & Duisburg
08.05.2020	7:00:00	11:50:00	BNJ	Hürtgenwald & FZJ
09.05.2020	7:29:00	15:23:00	BNJ– FDH	Hangelar-Stuttgart-Friedrichshafen
27.05.2020	7:22:00	12:00:00	FDH– BNJ	Friedrichshafen-Stuttgart-Bonn
29.05.2020	8:00:00	18:04:00	BNJ	Bonn-Köln-Düsseldorf-Mönchengladbach-Bonn
01.06.2020	7:00:00	16:28:00	BNJ	Bonn-Köln-Düsseldorf-Mönchengladbach-Bonn
02.06.2020	8:00:00	17:46:00	BNJ	Bonn-Köln-Düsseldorf-Mönchengladbach-Bonn
03.06.2020	6:30:00	11:15:00	BNJ	Bonn-Köln-Düsseldorf-Mönchengladbach-Bonn
11.06.2020	8:10:00	17:52:00	BNJ	Bonn-Köln-Düsseldorf-Mönchengladbach-Bonn
12.06.2020	7:35:00	18:00:00	BNJ	Bonn-Köln-Düsseldorf-Mönchengladbach-Bonn
13.06.2020	6:15:00	13:45:00	BNJ	Bonn-Köln-Bad Honnef-Bonn
15.06.2020	6:19:00	12:51:00	BNJ– FDH	Bonn-Bad Honnef-Friedrichshafen
02.09.2020	7:23:00	16:39:00	FDH	Friedrichshafen - Bodensee
03.09.2020	7:16:00	12:32:00	FDH– BNJ	Friedrichshafen-Bonn/Hangelar
06.09.2020	8:13:00	17:45:00	BNJ	Bonn - Bad Honnef - Köln - Bonn
07.09.2020	7:45:00	17:00:00	BNJ	Bonn - Bad Honnef - Köln - Bonn
08.09.2020	13:15:00	16:05:00	BNJ	Bonn - Bad Honnef - Köln - Bonn
10.09.2020	7:48:00	12:37:00	BNJ– BadH	Bonn - Frankfurt - Bad Homburg
11.09.2020	9:10:00	17:00:00	BadH	Bad Homburg - Frankfurt - Bad Homburg
12.09.2020	7:08:00	16:23:00	BadH	Bad Homburg - Frankfurt - Bad Homburg
13.09.2020	07:07:00	16:22:00	BadH	Bad Homburg - Frankfurt - Bad Homburg
14.09.2020	06:19:00	11:14:30	BadH– FDH	Ban Homburg - Friedrichshafen

FDH: Friedrichshafen, BNJ: Bonn-Hangelar, BadH: Bad Homburg airfield

110
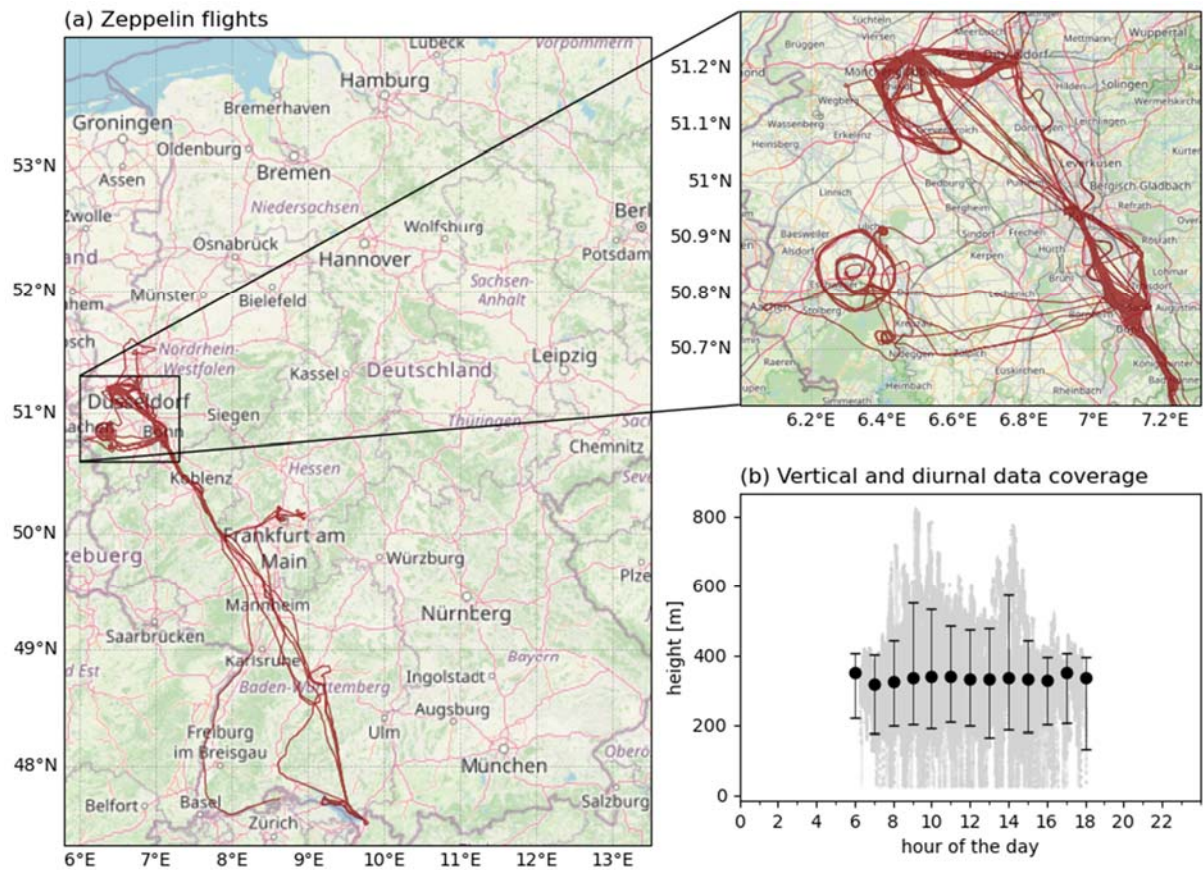
Figure 1: (a). The Zeppelin flight tracks over Germany (© OpenStreetMap contributors 2021. Distributed under the Open Data Commons Open Database License (ODbL) v1.0.) and (b). their vertical and diurnal coverage in UTC.

2.2 MIRO instrument

We deployed a MIRO MGA[10]-GP multi-compound gas analyzer, a newly available commercial instrument (MIRO Analytical AG, Wallisellen, Switzerland). The analyzer measures ten trace gases NO, NO_2, O_3, SO_2, CO, CO_2, CH_4, H_2O, NH_3, N_2O with a time resolution of 1s and precisions (1σ) as summarized in Table 2. The stated precisions were determined by Allan-Werle-Variance (Werle et al., 1993). A detailed description of the measurement principle and the instrument's data processing and characterization of the instrument can be found elsewhere (Liu et al., 2018, Hundt et al., 2018).

Table 2: Instrumentation onboard the Zeppelin airship.

Installation	Method	Parameter	Time resolution (response time)	Precision	Reference
Cabin Rack	Mid-infrared (MIR) direct laser absorption spectroscopy	O_3	1 s	± 0.6 ppb (1 σ)	MIRO AG
		NO		± 0.3 ppb (1 σ)	
		NO_2		± 0.04 ppb (1 σ)	
		CO		± 0.04 ppb (1 σ)	
		SO_2		± 1.7 ppb (1 σ)	
		NH_3		± 0.05 ppb (1 σ)	
		H_2O		± 12 ppm (1 σ)	
		CH_4		± 0.7 ppb (1 σ)	
		N_2O		± 0.08 ppb (1 σ)	
		CO_2		± 750 ppb (1 σ)	
Hatch box	Capacitive polymer sensor chip	RH	1s (4 s)	± 2 % RH	
		T	1 s (5 s)	± 0.3°C	
	Electrochemical sensor	NO	1 s (< 45 s)	± 15 ppb (2 σ)	Alphasense NO-B4
		CO	1 s (< 30 s)	± 0.6̶4 ppb (1̶–2 σ)	Alphasense CO-B4
		NO_2	1 s (< 80 s)	- ± 15 ppb (2 σ)̶±̶ ̶0̶.̶3̶ ̶p̶p̶b̶ ̶(̶1̶ ̶σ̶)̶	Alphasense NO2-B43F
		O_x ($NO_2 + O_3$)	1 s (< 80 s)	± 15 ppb (2 σ)̶ ̶±̶ ̶0̶.̶0̶4̶ ̶p̶p̶b̶ ̶(̶1̶ ̶σ̶)̶	Alphasense OX-B431
	Optical particle counter (0.3 – 10 µm)	Aerosol particles	1.3 s	-	Alphasense OPC- N3
	GPS	Latitude, Longitude, Altitude	5 s	-	NAVIN miniHomer 2.8

125

7

The instrument is a quantum cascade laser-based (QCL) spectrometer containing five distributed feedback (DFB) QCLs. The gas mixing ratios are measured by direct laser absorption spectroscopy of selected vibrational absorption lines of the target molecules. Beer-Lambert's law provides the relation between the light transmission and the mixing ratios of an absorbing species. To obtain the transmission spectra, the laser light is steered through an astigmatic Herriott cell to a Mercury Cadmium Telluride (MCT) detector. The Herriott cell is constantly flushed with the sampled gas providing an online in-situ measurement. The pressure in the cell was maintained at 95 hPa by means of using a pressure controller in combination with a membrane pump. The pulsing of the QCLs, the data acquisition, and spectral analysis are realized using custom-built electronics and software. The instrument's software runs on an integrated portable computer, which offers remote access and full remote control over the analyzer and its settings if an internet connection is provided. The instrument fits in a 19-inch rack, is four rack units (18 cm) high and 61 cm deep. An external membrane vacuum pump is used to pump air from the inlet through the analyzer. For temperature stabilization of the QCLs, an external water chiller is connected to the instrument that stabilizes the signal and reduces the noise of the measurements to minimize drifts caused by ambient temperature variations. For operation on the Zeppelin, the analyzer and its peripheral devices were integrated into a 19-inch rack as shown in Figure 2. During the Zeppelin flights, the instrument's inlet was switched to a zero-air supply of NO_x- and O_3-free air by sampling cabin air through zero air cartridges for 2 min every 20 min. The obtained zero points were used to apply a background correction to the NO, NO_2, and O_3 data to reduce their drift. For consecutive zero air measurements median background drift values were 0.56 ppb, 0.34 ppb and 2.9 ppb for NO, NO_2 and O_3, respectively. To test the instrument performance, zero air from a compressed gas cylinder was measured for 12 hours and the mixing ratios were determined by the laser spectrometer. The stated precisions were determined by Allan-Werle-Variance (Werle et al., 1993).

The instrument's software runs on an integrated portable computer, which offers remote access and full remote control over the analyzer and its settings if an internet connection is provided. For operation on the Zeppelin, the analyzer and its peripheral devices were integrated into a 19-inch rack as shown in Figure 2. The instrument is four rack units (18 cm) high and 61 cm deep. The sample inlet line connected to the MIRO consisted of an unheated 8 m long PFA (perfluoroalkoxy alkane) tube with an internal diameter of 4 mm. The sample air was drawn from the inlet located at the hatch box below the Zeppelin cabin at a flow rate of 1.2 lpm resulting in a residence time of around 5 s.

The performance of the MIRO with its sampling line to measure sticky molecules including NH_3 and H_2O was further examined by laboratory measurements which mimicked the conditions during the Zeppelin flights. Fast changes of pollutant concentrations were applied to determine the response times (t_{90}) of the measurement system, which were 240 s and 9 s for NH_3 and H_2O, respectively (see Figure S1). This highlights the future need for a heated sampling line in order to provide quality assured data, especially for NH_3. We therefore omitted NH_3 from our discussion. For H_2O and less sticky molecules response times below 9 s result in a spatial horizontal resolution of < 150 m considering a horizontal Zeppelin flight speed of 60 km/h and a vertical resolution of < 15 m for a vertical speed of 1.7 m/s. This provides the upper limits of the spatial resolution of pollutant concentration but is sufficient for the analysis included in this work. Finally, the instrument detection

limit for SO_2 is 1.7 ppb i.e., 4.9 µg/m³ (1 σ) and the expected SO_2 concentrations in European urban areas are mostly below 5 µg/m³ (Henschel et al., 2013). Therefore, SO_2 measurements are omitted from further discussions within this paper.

Figure 2: Instrumentation onboard the Zeppelin aircraft. **(**Zeppelin picture by Michael Häfner**)**

2.3 Hatch box for low-cost sensors and optical particle counter

Figure 2 and Figure ~~S1~~ S2 show the hatch box arrangement for multiple sensors deployed below the Zeppelin cabin. Six setups were installed each including an amperometric electrochemical gas sensor (ECS) for CO, NO, NO_2, and O_X (O_3 + NO_2) measurements (Baron and Saffell, 2017), a ChipCap2 sensor for temperature (T) and relative humidity (RH) measurements, and a GPS locator for latitude, longitude and altitude measurements. Particle-phase size distribution measurements were performed by two optical particle counters (OPCs). Currently, the optical counter has been used based on the available instrument recommendations with and without an isokinetic inlet. The isokinetic inlet has been a 3-D-printed L-shaped inlet of 10 cm length and an internal diameter of 5 mm. The second OPC was used without any inlet line, sampling perpendicular to the flight direction. No further sample preparation or quality assurance has been performed. We therefore exclude the OPC data in its current state from further discussion. Two Long Term Evolution (LTE) antennas were used for real-time communication to the instruments from the ground and wireless communication for onboard decisions. Details on the performance of the sensors including their time resolution, the limit of detection, and references are found in Table 2. Furthermore, the potential of the ECSs to measure nitrogen oxides is shown in Figure S3. On average, ECS NO_X data are higher by 20% compared to the MIRO for concentrations above 15 ppbv which is the limit of detection for NO_X measured by ECS. This makes the ECSs ideal for the identification of high NO_X emission

sources during the Zeppelin flights but limited in determining NO_x variability at low-NO_x environments. Calibrations, sensitivity analysis, and associated uncertainties of the ECSs measurements will be further discussed in a separate publication and are not the focus of this work. In the following, all measured pollutant concentrations are acquired from the MIRO instrument.

2.5 4 The EURAD-IM model

The EURAD-IM model output was compared to the Zeppelin observations by focusing on the emissions and evolution of an industrial plume as discussed in section 3.4. Details of the model are provided by Elbern et al. (2007). Briefly, the regional emission inventory provided by the Copernicus Atmosphere Monitoring Service (CAMS) (Kuenen et al., 2014) was used and further refined using land use information. The Weather Research and Forecasting (WRF) model version 4.0.3 (Skamarock et al., 2008, Powers et al., 2017) was initialized using the global analysis of the European Centre for Medium-Range Weather Forecasts (ECMWF) to account for the meteorological effects whereas the RACM-MIM chemical mechanism (Pöschl et al., 2000) was applied to account for the effects of atmospheric chemistry on pollutant concentrations. Here, we focus on 1-h time resolution model concentrations for NO_x NO_x and CO on a 1 km horizontal grid. The observational average flight height during the comparison periods was around 300 m and the model level centered at about 268 m was chosen as the closest vertical grid point in proximity to these measurements. A challenge in accurately determining the location of different emission sources in the model is that the horizontal resolution of the inventory emissions is coarser (approx. 7 km in Western Germany) than the model resolution (1 km). When refining the emissions to match the model grid, it is often hard to match single emission patterns with an operational forecast model. This was the case for the modeled industrial emission source investigated in section 3.4 that was offset by 3 km to the southeast compared to the original location of the power plant. Here, NO_x concentration fields that are associated with the significant point source were reallocated to match the location of the industry and improve the comparison to observations. Reallocation of the CO concentrations was not applied since this studied power production facility had negligible CO emissions. CO background concentrations were variable due to the numerous other point sources and the longer CO lifetime.

3 Results and Discussion

3.1 Vertical profiles in Frankfurt and Bonn

Zeppelins can climb and descend slowly at confined locations to obtain the vertical distribution of pollutants. Each day, multiple flights were performed with vertical measurements obtained during the Zeppelin landing and take-off at the airports. Figure 3 shows the vertical profiles of NO_x NO_x and O_3 at different times of the day for measurements performed nearby Frankfurt in September and Bonn in May, June, and September. For Bonn, larger variability in pollutant concentrations due to the broader seasonal coverage was not evident with measurements in May and June showing on average similar vertical trends as in September (Figure S2 S4). Zeppelin data below 25 m were excluded from the analysis as they were affected by the Zeppelin engine exhaust emissions. In the early hours from 06:00 to 08:00 UTC, NO_x NO_x mixing ratios close to the ground were higher with a median (25th–75th percentile) of 8 (5–19) ppbv and 5.7 (3–20) ppbv for Frankfurt and Bonn, respectively. In Frankfurt, the median NO_x NO_x concentration sharply decreased down to 1 (0.27–6) ppbv when above 125 m, whereas in

225 Bonn, a moderate decrease to 5 (2.7–10) ppbv was observed. O_3 showed the opposite trend with low mixing ratios close to the ground and an O_3 increase above 125 m in height. During the period from 08:00 to 10:00 UTC, an increase of ~~NO_x~~ NO_x at all heights compared to 06:00 UTC was evident in Frankfurt, whereas in Bonn, ~~NO_x~~ NO_x was similar to earlier hours with a slight increase of ground-level ~~NO_x~~ NO_x to 9.2 (3.1–14.5) ppbv. In parallel, O_3 decreased at higher altitudes and increased closer to the ground for Frankfurt and Bonn compared to earlier hours.

230 From 10:00 to 18:00 UTC, the lower PBL was well mixed with ~~NO_x~~ NO_x and O_3 concentrations agreeing within their variability at all heights from 25 m up to 375 m. ~~NO_x~~ NO_x concentrations decreased throughout the day down to less than 1 ppbv, whereas O_3 increased up to more than 60 ppbv for both Frankfurt and Bonn. Same trends were observed for other criteria pollutants including CO, CO_2, and CH_4 (Figure ~~S3~~S5), whereas N_2O, H_2O, and NH_3 were less variable (Figure ~~S4~~S6).

11
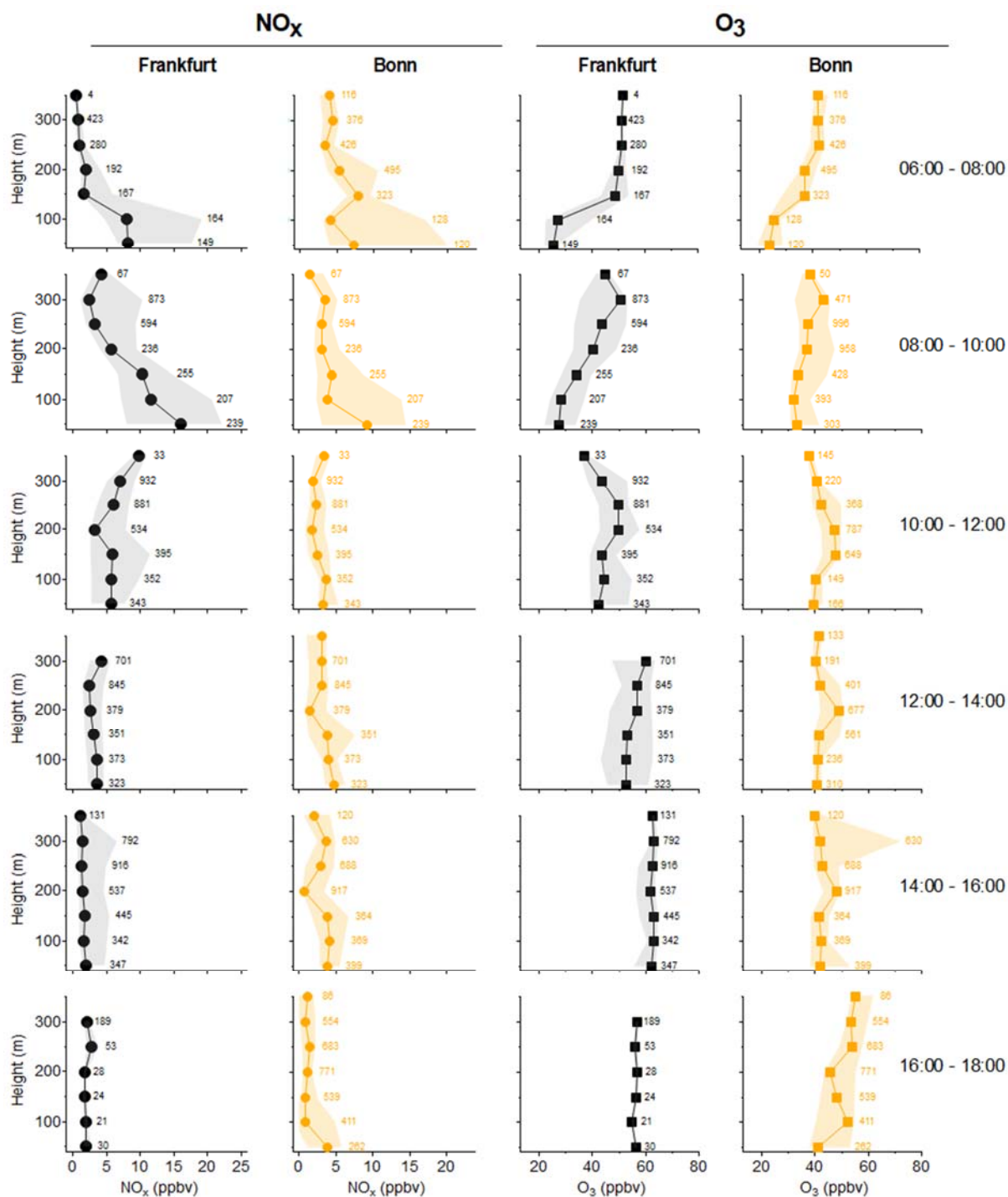
Figure 3: Vertical profiles for different time-periods (UTC) for ~~NOx~~-NO_x and O_3 in Bonn and Frankfurt. Circle and square markers correspond to the median ~~NOx~~-NO_x and O_3 mixing ratios, respectively. The shaded areas represent the 25th and 75th percentiles. Numbers correspond to the data points used to generate the ~~NOx~~-NO_x and O_3 medians.

Changes in PBL dynamics, anthropogenic emissions, and atmospheric chemistry are the drivers of the observed diurnal and vertical variability. During nighttime, a shear develops between the residual layer and the more stagnant nocturnal boundary layer that grows higher and reaches a morning maximum. (see Figure ~~S5~~S7). Shortly after sunrise, the surface heats up and a mixed layer evolves increasing with height until the former nocturnal boundary layer and the residual layer are finally fully mixed. From 08:00 to 10:00 UTC, the Zeppelin captured

the evolving convective mixed layer that developed after sunrise and reached on average up to 125 m. The increased ground-level NO_x concentrations during the early hours are the result of fresh emissions from ground sources into a shallow mixed layer. As the convective mixed layer increases, ground-level NO_x concentrations are expected to decrease due to dilution effects. Higher altitude concentrations increase as more concentrated ground-level NO_x is distributed vertically. The morning anthropogenic emissions including rush-hour traffic increase the ground-level NO_x but dilution mitigates the level of NO_x concentrations at low altitudes in Frankfurt and Bonn during the morning hours. O_3 is a secondary product from the interplay of NO_x, volatile organic compound emissions, and meteorology. Under dark conditions, O_3 is expected to react away and its concentration decreases, whereas during the day, it is expected to reach maximum concentrations midday when photochemistry peaks. These trends are verified by the Zeppelin flights in Frankfurt and Bonn where early morning O_3 titration is followed by photochemical O_3 production/increase midday with uniform vertical distributions obtained after 10:00 UTC.

3.2 NO_x vertical profiles compared to ground-based monitoring stations

The above field-derived vertical profiles show the influence of PBL dynamics in diluting pollutant concentrations but also highlight the influence of anthropogenic emissions. Comparison of these profiles to ground-based measurements provides insights into their origin and location. Figure 4 compares the NO_x vertical profiles in Frankfurt to ground-based observations from various monitoring stations (provided by Unweltbundesamt, Table S1). Twelve ground-based monitoring stations were chosen located in the broader Frankfurt metropolitan area as shown in Figure 4a. Monitoring stations in the inner city namely, Frankfurt-Höchst, Frankfurt-Niedwald, Frankfurt-Ost, Frankfurt-Schwanheim, Frankfurt-Friedberger Landstraße, and Offenbach-Untere Grenzstraße are categorized as urban. Monitoring stations in the outer Frankfurt area including Hanau, Raunheim, Wiesbaden-Süd, Wiesbaden-Ringkirche, and Wiesbaden-Schiersteiner Straße were categorized as suburban. Finally, Kleiner Feldberg was considered a remote station at a higher altitude, 700 m above the city center of Frankfurt and 300-400 m above the Zeppelin flight track. Figure 4b shows a detailed comparison of the NO_x diurnal variability of the ground stations and the Zeppelin measurements. For the urban and suburban stations, a NO_x peak was evident with an average ($\pm$ 1σ) concentration of 46.3 ($\pm$ 4.9) ppbv and 35.6 ($\pm$ 10.1) ppbv in the morning hours. Midday, the NO_x concentrations decreased due to the increasing convective mixed layer height as well as reduced traffic emissions and increased again in the evening due to rush-hour traffic reaching a maximum of 56.6 ($\pm$ 25) ppbv and 41.3 ($\pm$ 23.7) ppbv for the urban and suburban stations, respectively. At the remote station, the NO_x concentrations were at background levels and no significant anthropogenic contribution was evident. Zeppelin data followed the same morning increase as the urban and suburban monitoring stations with maximum NO_x at 21.7, 21.3, 11.4, and 5 ppbv for measurements at 50, 100, 150, and 200 m, respectively, during the time from 08:00–10:00 UTC. For higher altitude measurements at 250 and 300 m, the NO_x concentrations were the highest from 10:00–12:00 UTC with concentrations of 6.3 and 8.85 ppbv, respectively.

At lower altitudes, Zeppelin flew close to the outer urban airfield while at higher altitudes it was located closer to the city center of Frankfurt as shown in Figure 4a. It is therefore expected that measurements taken at low altitudes are comparable to those from suburban monitoring stations in particular during the early morning hours when the convective mixing layer starts evolving and the dilution of fresh emissions is less pronounced. However, ground-

based (sub-)urban stations are located close to roads or even in road canyons catching fresh emissions and observed concentrations of primary emissions were higher on average than the respective low altitude Zeppelin data (Figure 4b). In the morning hours, the effect of rush hour traffic emissions on both the Zeppelin and urban/suburban stations is evident with a peak in ~~NO$_x$~~ NO$_x$ concentrations at altitudes below 200 m at 08:00–10:00 UTC. For higher altitude measurements (250–300 m) the NO$_x$ concentrations peak at 10:00–12:00 UTC which highlights the effect of PBL dynamics where morning emissions are distributed vertically to generate a well-mixed layer, resulting in a~~and the~~ dilution ~~process~~ of the mixed air masses. This results in a later and weaker peak of the NOx concentration ~~in the~~at high altitudes. ~~This observed change in dynamics cease with~~As the convective layer reach~~ing~~es altitudes above the upper flight range of the Zeppelin, this observed change in dynamic is no longer captured. In the afternoon, no significant concentration differences are observed between the different heights. The evening peak captured by the monitoring stations is only partially measured by the Zeppelin. Future Zeppelin campaigns to capture the nocturnal boundary layer development in the evening hours will provide further insights into the diurnal variability of the PBL.

These results provide evidence of effective vertical mixing in particular during the afternoon but limited to the heights captured by the Zeppelin. Future studies to convey whether mixing is as efficient at higher altitudes, that has been previously achieved by aircraft studies (e.g., Flynn et al., 2014; Flynn et al., 2016; Choi et al., 2020; Li et al., 2021), will be of great interest. Furthermore, comparison of the Zeppelin flights not only to ground-based monitoring stations, but also to modeling efforts as well as satellite measurements, would be of great value as geostationary satellites come on-line in the future.
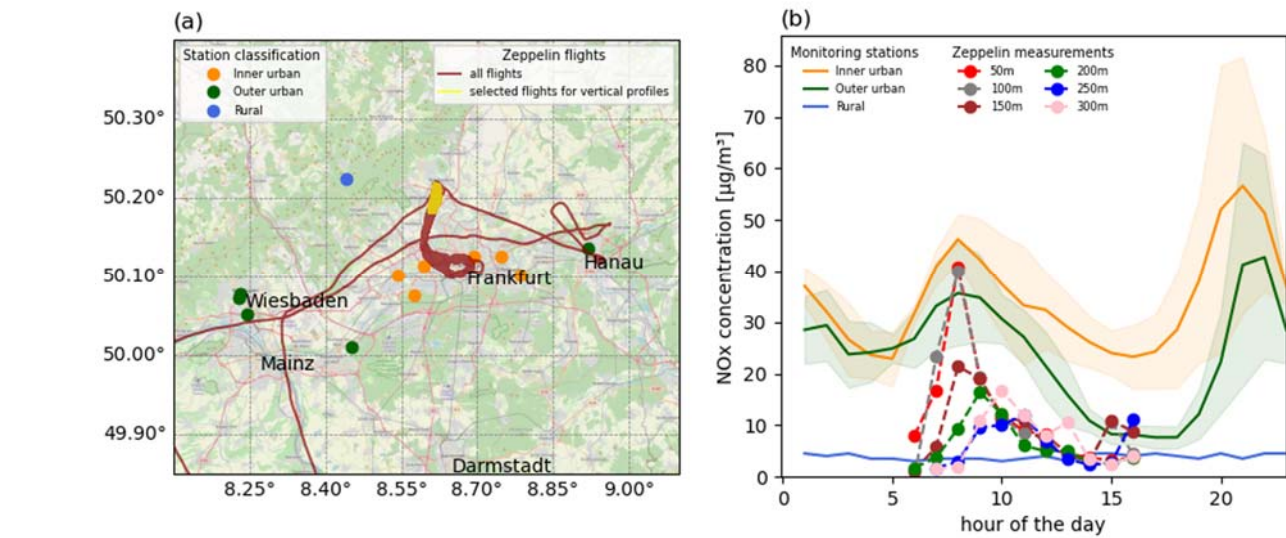
Figure 4: a. The map of Frankfurt overlaid with the Zeppelin flight tracks in red and yellow that are ~~(~~used to generate the vertical profiles shown on the right~~)~~. Multiple flight paths to the city center of Frankfurt are overlayed and appear as a thick red line. ~~, an~~Also shown is ~~d~~the urban, suburban, and remote monitoring station locations with brown, green, and blue circle markers, respectively (Data provided by the Umweltbundesamt). (© OpenStreetMap contributors 2021. Distributed under the Open Data Commons Open Database License (ODbL) v1.0.) b. Average diurnal ~~NOx~~ NO$_x$ concentration profiles for the urban, suburban, and remote monitoring stations and the Zeppelin diurnal profiles at different heights.

3.3 Comparison to the EDGAR 2015 emission inventory

Airborne Zeppelin measurements are an ideal platform to investigate pollutant concentrations on the vertical; however, the majority of flight hours were at heights ranging from 250-450 m. During these periods, the Zeppelin flew over various cities, including Cologne, Mönchengladbach, Düsseldorf, Aachen, Frankfurt, but also over industrial areas, and highways. This provided the opportunity to better characterize anthropogenic emissions and compare observations to emission inventory estimates for Germany. Here, we use the 2015 Emissions Database for Global Atmospheric Research (EDGAR v5) (Crippa et al., 2020), which is the most recent year for which data are publicly available. Emissions in EDGAR are provided in Gg/year while pollutant concentrations detected onboard the Zeppelin are measured in ppbv. A direct comparison of the emission inventories and observations is challenging. From emission to detection, measured pollutant concentrations can drastically change due to dilution as well as chemical and physical loss processes whereas the annual inventory emission estimates may differ from daily or even hourly emission rates. A common strategy to reduce the above described uncertainties has been to focus on pollutant mass ratios (Gkatzelis et al., 2021b; Coggon et al., 2021). For example, if CO and a volatile organic compound are co-emitted from a pollution source their ratio is constant as they travel downwind of the source if their physical and chemical loss pathways are not different and provided they do not have other sources.

Figure 5 shows the diurnal variability of the NO_x to CO slope for all Zeppelin flights between 250 m and 450 m. A sensitivity analysis was performed to derive the observed NO_x to CO slope by applying a linear fit function every 60 s, 100 s, or 1000 s. Linear fits obtained from each time step were further filtered depending on the goodness of fit with data discarded if the coefficient of determination R^2 of the linear fit was below 0.6, 0.7, or 0.8, respectively. An overview of this sensitivity analysis to the different time steps and R^2 thresholds is given in Figure S8. Overall, the NO_x to CO slopes were within $\pm$ 0.05 g g^{-1} independent of the chosen time steps and R^2 thresholds. Therefore, for Figure 5 we choose a 1 min time step and an R^2 threshold of 0.6 to discuss the observed variability of the NO_x to CO slopes. Figure 5 also shows the NO_x to CO emission ratios from numerous pollution sources based on the EDGAR 2015. The EDGAR emission inventory was separated into different emission sectors including transportation, industry, building and miscellaneous, and other sources by lumping the IPCC emission categories. Road transportation with no resuspension is the dominant source of NO_x in the inventory accounting for 40 % of the NO_x emitted in Germany with a NO_x/CO ratio of 0.68 g/g. Other transportation categories are not expected to contribute more than 6 % to the total NO_x emissions, however they have drastically higher NO_x/CO ranging from 3–10 g/g. Industrial emissions are dominated by the categories "main activity electricity and heat production" and "manufacturing industries and construction" accounting for 22 % and 18 % of the total NO_x, with NO_x/CO at 1.37 and 0.56, respectively. The remaining industrial emissions account for 3 % of the total NO_x and their NO_x/CO ranges from 0.017–24.32 g/g. Building and miscellaneous sources account for 11 % of the total NO_x in EDGAR and are predominantly related to residential emissions and off-road vehicles with NO_x/CO at 0.08. NO_x to CO slopes during the Zeppelin flights were relatively constant with a daily average of 0.36 ($\pm$ 0.03) g/g. These values were in the range of the average emission ratio of road transportation, building and miscellaneous emissions, and specific industrial sources when compared to EDGAR 2015. Higher NO_x to CO levels by a factor of 2 to 5 compared to the daily average were evident promoting sporadic detection of high NO_x emission sources

15

350 compared to CO. Figure 6 shows that the spatial distribution of these higher NO_x-NO_x to CO emissions is predominantly related to petroleum refinery and chemical industries along the flight tracks in North Rhine Westphalia and Hessen further promoting the potential of Zeppelin flights to locate different pollution sources in space and time. A characteristic example of higher NO_x-NO_x to CO industrial emissions is highlighted in section 3.4 and further investigation of individual emission sources is the focus of a future study.
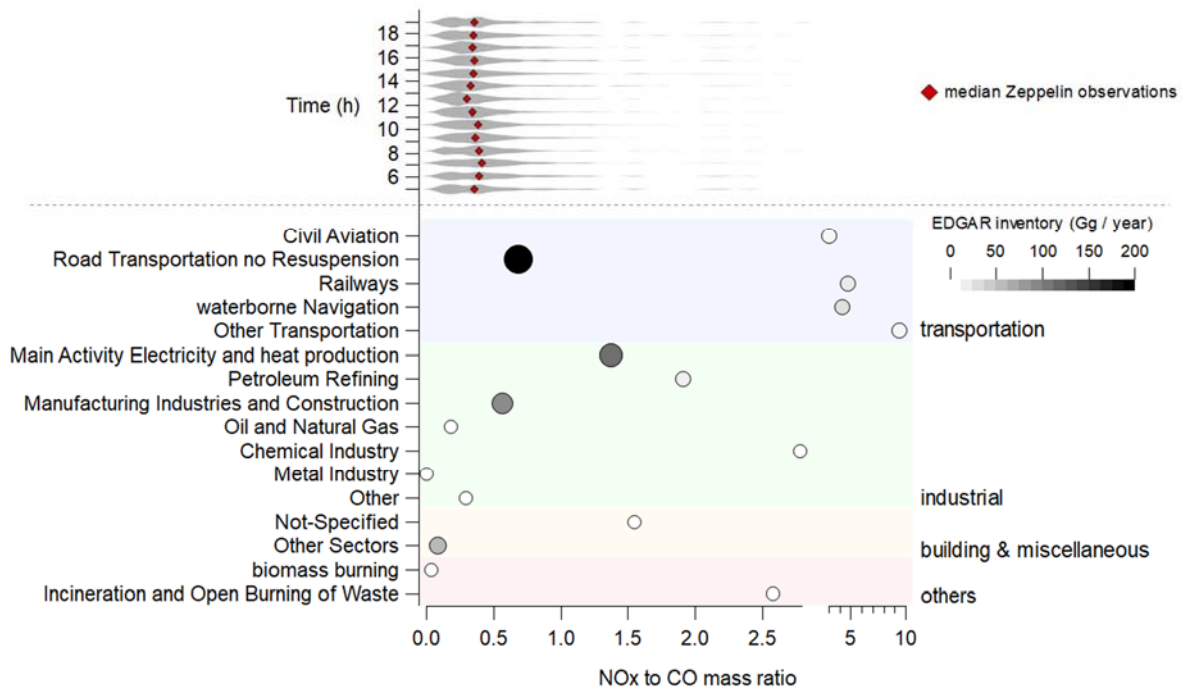
355

Figure 5: Distribution of the NO_x-NO_x to CO ratio (g / g) during the Zeppelin flights shown as a violin plot for measurements ranging from 250 to 450 meters in height. These ratios are compared to the ratios of different pollution sources following the EDGAR 2015 emission inventory. The size and color of the markers indicate the NO_x-NO_x emission strength for each EDGAR source.

16
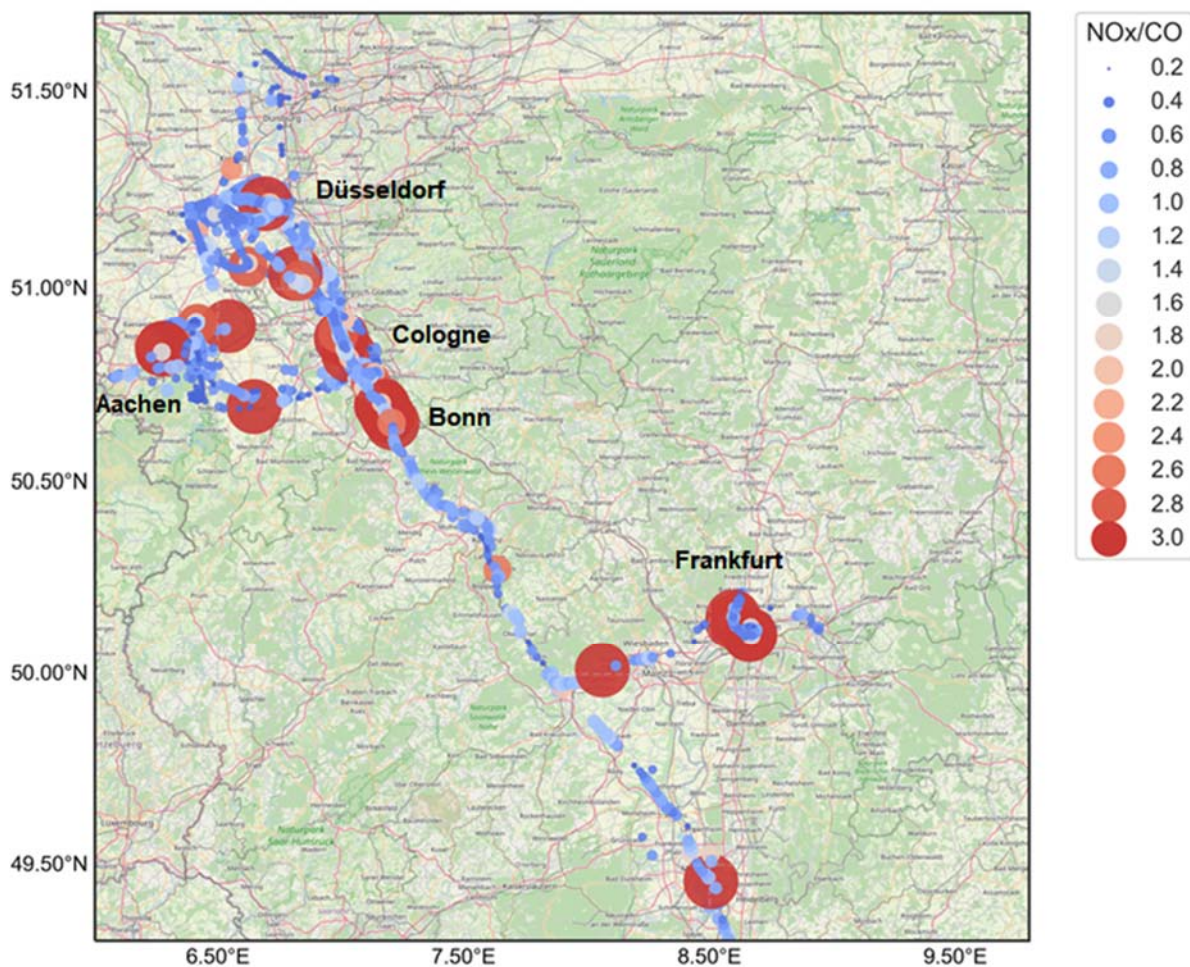
Figure 6: Identified areas of high NO$_x$ relative to CO emissions in Germany during the Zeppelin flights (© OpenStreetMap contributors 2021. Distributed under the Open Data Commons Open Database License (ODbL) v1.0.).

The observed ~~NO$_x$~~NO$_x$/CO slope can be influenced by the longer lifetime of CO compared to ~~NO$_x$~~ NO$_x$ (Seinfeld, 2006) and therefore bias the measurements low. The longer CO lifetime also leads to higher background levels; however, when focusing on the ~~NO$_x$~~NO$_x$/CO slope this background is accounted for in the offset of the linear fit. The major ~~NO$_x$~~NO$_x$ daytime loss pathway is the reaction of NO$_2$ with the OH radical yielding nitric acid. The net chemical loss of ~~NO$_x$~~NO$_x$ in the atmosphere is challenging to directly observe. Observational methods to determine the lifetime of ~~NO$_x$~~NO$_x$ have shown that under typical midday conditions in an isoprene-dominated forest it was 11 h ± 5 h (Romer et al., 2016), whereas for studies focused on the outflow of isolated emissions the average range of ~~NO$_x$~~NO$_x$ lifetimes was around 5-8~~7~~ h (Ryerson et al., 1998; Liu et al., 2016; Dillon et al., 2002; Alvarado et al., 2010; Valin et al., 2013). The vertical trajectory time for emissions to be detected onboard the Zeppelin is expected to be below the above lifetime thresholds due to the midday vertical mixing with vertical wind speeds in the range of 1 to 2 m/s (Stull, 1988). However, the net chemical loss of ~~NO$_x$~~NO$_x$ cannot be neglected, especially if shorter NOx lifetimes are evident due to the efficient production of multifunctional nitrates (e.g., Valin et al., 2013). Therefore, ~~and~~ the observational ratios presented here are a lower estimate compared to the ratios close to the emission source.
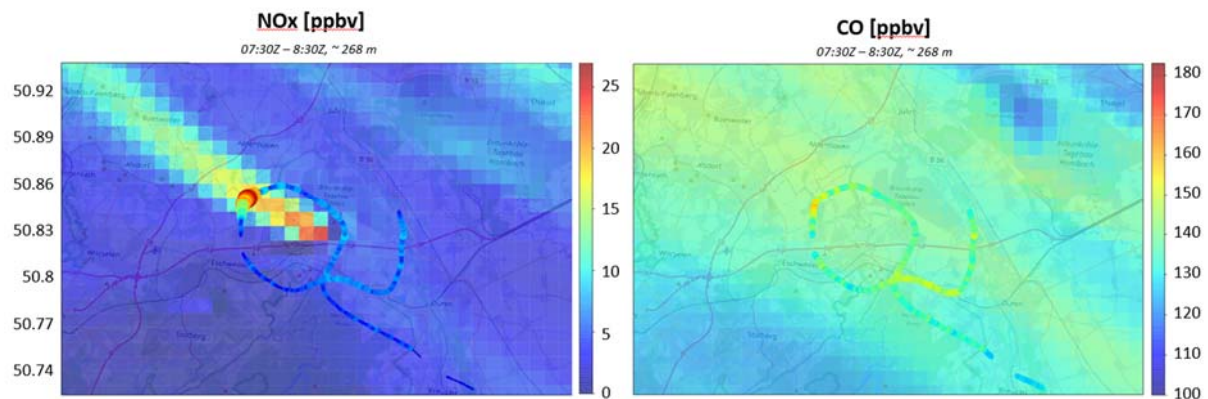
17

Uncertainties can also exist in the 2015 EDGAR emission inventory estimates compared to the expected emissions in 2020 when the Zeppelin flights were performed. The European Environmental Agency reports a drastic

380   decrease in ~~NOx~~ NO_x emissions by more than 60% from 1990 to 2017 (EEA, 2019). Assuming the decrease in ~~NOx~~ NO_x emissions is stronger compared to the decrease of CO from 2017 to 2020, this could lead to an overestimation of the EDGAR ~~NOx~~ NO_x/CO ratios presented here. Furthermore, 2020 was the year that the COVID-19 pandemic led to unprecedented government restrictions to limit the spread of the disease. Gkatzelis et al. (2021a) show that reduced ~~NOx~~ NO_x and CO emissions correlate with stricter government responses that could

385   affect the ~~NOx~~ NO_x and CO observations. Although transportation and industrial emissions are expected to decline during lockdown conditions, building emissions could have risen. The increased contribution of building emissions could therefore explain why observational ~~NOx~~ NO_x/CO ratios fall along with the EDGAR transportation/industry and building emission ratios.

3.4 Targeted flights to identify coal power plant emissions

390   As highlighted in the previous section, emissions from industrial energy production are a major contributor to pollutant concentrations in Germany. Industrial pollution sources were identified in proximity to the Zeppelin airports using the EURAD-IM model prior to flights performed in North Rhine-Westphalia. The coal power plant in Weisweiler (50.838° N, 6.321° E) was chosen to investigate the vertical and horizontal evolution of industrial emissions on May 8, 2020, at 06:00-14:00 UTC.

395   Figure 7 shows the EURAD-IM model results (see section 2.4) for ~~NOx~~ NO_x and CO concentrations overlaid with observations on-board the Zeppelin for one transect crossing the industrial plume at 7:30-8:30 UTC. Comparison of the EURAD-IM model and observations at different industrial plume heights and different time periods are the focus of future work; here we highlight the potential of Zeppelin measurements as valuable input for model evaluation or data assimilation approaches. EURAD-IM ~~NOx~~ NO_x concentrations were at 25 ppbv close to the

400   industrial emissions and decreased moving downwind of the industry due to dilution. The Zeppelin flew in circles around the industry during the same period. NO_x background concentrations were at 5-10 ppbv and increased to 10-25 ppbv when flying through the industrial plume. Model concentrations ranged from 5 to 10 ppbv upwind of the industry location in the southern and eastern regions and were in good agreement with observational trends. The model NO_x concentrations were on average 18-20 ppbv for this industry and agreed within 12% with the

405   Zeppelin measurements for this transect. Industrial CO emissions were minimal both in the model and observations and background CO levels agreed within less than 10%.

Figure 7: Evolution of industrial plume emissions of NO_x and CO based on the EURAD-IM model overlaid by the field-derived Zeppelin observations.

Industrial emissions during the period of the measurements were lower than the business-as-usual emission scenario due to the increased contribution of solar and wind energy (Energy-Charts) and/or the impact of lockdown measures. Particularly, the net electricity generation from the Weisweiler coal power plant during the Zeppelin flight was 50% less compared to the weekly average generation for 2020 ~~(Figure S7)~~. The good agreement between the model and observations for NO_x concentrations could therefore be due to an overestimation of NO_x emissions at this given time by the model. However, the model NOx and CO background concentration levels are in good agreement with observations. Although the period of the measurements was during lockdown conditions, the background NO_x and CO levels seem to be unaffected by the stay-at-home orders.

4 Conclusions

We report in-situ measurements of air pollutant concentrations within the planetary boundary layer on board the Zeppelin NT airship in Germany. A novel quantum cascade laser-based multi-compound gas analyzer (MIRO Analytical AG) is deployed to simultaneously measure the concentration of greenhouse gases (CO_2, N_2O, H_2O, and CH_4) and air pollutants (CO, NO, NO_2, O_3, SO_2, and NH_3) with high precision at a measurement rate of 1 Hz. Electrochemical sensors for NO, NO_2, O_x (NO_2+O_3), and CO, an optical particle counter, temperature, humidity, altitude, and position monitoring are attached to a hatch box below the Zeppelin cabin. In total, 14 commercial flights, 4 targeted flights, and 6 transect flights are performed in May, June, and September 2020, and include flights over urban, remote, but also industrial areas, and highways.

Vertical profiles of pollutants are obtained with a focus on ~~NOx~~ NO_x and O_3 during the airship landing and take-off close to the airports of Bonn and Frankfurt. In the early hours from 06:00 to 08:00 UTC, ~~NOx~~ NO_x mixing ratios are higher close to the ground and sharply decrease when above 125 m. O_3 has the opposite trend with low mixing ratios close to the ground and an O_3 increase above 125 m. This is due to a developing convective mixing layer in which dilution of fresh emissions is less pronounced leading to an increase in ~~NOx~~ NO_x concentrations close to the ground, and the subsequent titration and decrease of ground-level O_3. From 08:00 to 10:00 UTC, an increase of ~~NOx~~ NO_x mixing ratios is evident at all heights due to the morning rush hour traffic emissions. From

19

10:00 to 18:00 UTC, the convective mixing layer is fully developed within the max. flight height of 450 m above ground and well mixed with NO_x-NO_x and O_3 concentrations agreeing within their variability at all heights. During these periods, NO_x-NO_x concentrations decrease throughout the day due to vertical dilution whereas O_3 increases due to increased photochemical activity. We compare the diurnal variability of the Zeppelin vertical profiles to measurements from ground-based monitoring stations in Frankfurt to find that Zeppelin vertical concentrations are predominantly affected by suburban emissions and only the higher altitude measurements are influenced by urban Frankfurt emissions.

NO_x-NO_x to CO slopes at higher altitudes (250–450 m) are compared to the 2015 EDGAR emission inventory. A daily average of 0.36 (± 0.03) g/g is found for the Zeppelin measurements in the range of the inventory emission ratios for transportation, residential emissions, manufacturing industries, and construction activity. Sporadic high NO_x-NO_x to CO slopes (2-5 g g^{-1}) close to industrial sources are observed including a coal power plant in Weisweiler. We compare dedicated measurements in this industrial facility to the EURAD-IM model to find agreement within less than 15% for NO_x-NO_x and CO concentrations during one plume transect. However, due to the increased contribution of solar and wind energy and/or the impact of lockdown measures the power plant was operated at 50% capacity; therefore, possible overestimation of emissions by the model cannot be excluded. Nevertheless, an agreement between the model and observations for background NO_x-NO_x and CO concentrations promotes that emissions were not drastically affected due to lockdown restrictions as they are adequately represented by the model calculations, in which no emission reductions to account for the lockdown have been included.

From obtaining vertical pollutant distributions to evaluating emission inventories and modeling efforts the findings of this work highlight the unique scientific insights obtained aboard a Zeppelin platform and promote the importance of frequent airship measurements in Europe in the following years. Furthermore, the low costs of commercial flights provide an affordable and efficient method to improve our understanding of changes in emissions in space and time. Future efforts to include volatile organic compound measurements along with the greenhouse gases and air pollutants obtained by the MIRO MGA[10]-GP multi-compound gas analyzer will further expand the capabilities of this platform and provide insights into primary and secondary pollution observations.

Data availability

Tillmann, Ralf, 2022, "Replication Data for: Zeppelin flights 2020: Air quality observations", https://doi.org/10.26165/JUELICH-DATA/7ZZIXJ

Author contribution

RT, FR and AKS designed the experiments and flight campaigns. BW, CW, TS and FR carried them out. OA and MH provided profound instrumentation support AL, PF and EF provided the model data. GIG, TS and MD visualized the data. GIG and RT prepared the manuscript with contributions from all co-authors. RW, FR, PF and AKS commented on the manuscript.

Acknowledgments

475

The authors declare that they have no conflict of interest.

References

480 Alvarado, M. J., Logan, J. A., Mao, J., Apel, E., Riemer, D., Blake, D., Cohen, R. C., Min, K. E., Perring, A. E., Browne, E. C., Wooldridge, P. J., Diskin, G. S., Sachse, G. W., Fuelberg, H., Sessions, W. R., Harrigan, D. L., Huey, G., Liao, J., Case-Hanks, A., Jimenez, J. L., Cubison, M. J., Vay, S. A., Weinheimer, A. J., Knapp, D. J., Montzka, D. D., Flocke, F. M., Pollack, I. B., Wennberg, P. O., Kurten, A., Crounse, J., Clair, J. M. S., Wisthaler, A., Mikoviny, T., Yantosca, R. M., Carouge, C. C., and Le Sager, P.: Nitrogen oxides and PAN in

485 plumes from boreal fires during ARCTAS-B and their impact on ozone: an integrated analysis of aircraft and satellite observations, Atmos. Chem. Phys., 10, 9739-9760, https://doi.org/10.5194/acp-10-9739-2010, 2010.

Baron, R., and Saffell, J.: Amperometric Gas Sensors as a Low-Cost Emerging Technology Platform for Air Quality Monitoring Applications: A Review, ACS Sensors, 2, 1553-1566, 10.1021/acssensors.7b00620, 2017.

490

Benedict, K. B., Zhou, Y., Sive, B. C., Prenni, A. J., Gebhart, K. A., Fischer, E. V., Evanoski-Cole, A., Sullivan, A. P., Callahan, S., Schichtel, B. A., Mao, H., Zhou, Y., and Collett Jr, J. L.: Volatile organic compounds and ozone in Rocky Mountain National Park during FRAPPÉ, Atmos. Chem. Phys., 19, 499-521, https://doi.org/10.5194/acp-19-499-2019, 2019.

495

Boschetti, F., Chen, H., Thouret, V., Nedelec, P., Janssens-Maenhout, G., and Gerbig, C.: On the representation of IAGOS/MOZAIC vertical profiles in chemical transport models: contribution of different error sources in the example of carbon monoxide, Tellus B: Chemical and Physical Meteorology, 67, 28292, https://doi.org/10.3402/tellusb.v67.28292, 2015.

500

Cai, W., Li, K., Liao, H., Wang, H., and Wu, L.: Weather conditions conducive to Beijing severe haze more frequent under climate change, Nature Climate Change, 7, 257-262, https://doi.org/10.1038/nclimate3249, 2017.

505 Choi, S., Lamsal, L. N., Follette-Cook, M., Joiner, J., Krotkov, N. A., Swartz, W. H., Pickering, K. E., Loughner, C. P., Appel, W., Pfister, G., Saide, P. E., Cohen, R. C., Weinheimer, A. J., and Herman, J. R.: Assessment of NO2 observations during DISCOVER-AQ and KORUS-AQ field campaigns, Atmos. Meas. Tech., 13, 2523-2546, 10.5194/amt-13-2523-2020, 2020.

510 Coggon, M. M., Gkatzelis, G. I., McDonald, B. C., B.Gilman, J., H.Schwantes, R., Abuhassan, N., Aikin, K. C., Arendde, M. F., Berkoff, T. A., Brown, S. S., Campos, T. L., Dickerson, R. R., Gronoff, G., Hurley, J., Isaacman-VanWertz, G., Koss, A. R., Li, M., A.McKeen, S., Moshary, F., Peischl, J., Pospisilova, V., Ren, X., Wilson, A., Wude, Y., Trainer, M., and Warneke, C.: Volatile chemical product emissions enhance ozone and modulate urban chemistry, Proceedings of the National Academy of Sciences, 118, 32, https://doi.org/10.1073/pnas.2026653118, 2021

515

Crippa, M., Solazzo, E., Huang, G., Guizzardi, D., Koffi, E., Muntean, M., Schieberle, C., Friedrich, R., and Janssens-Maenhout, G.: High-resolution temporal profiles in the Emissions Database for Global Atmospheric Research, Scientific Data, 7, 121, e, 2020.

520 Crosman, E. T., Jacques, A. A., and Horel, J. D.: A novel approach for monitoring vertical profiles of boundary-layer pollutants: Utilizing routine news helicopter flights, Atmospheric Pollution Research, 8, 828-835, https://doi.org/10.1016/j.apr.2017.01.013, 2017.

Dang, R., Yang, Y., Hu, X.-M., Wang, Z., and Zhang, S.: A Review of Techniques for Diagnosing the
525 Atmospheric Boundary Layer Height (ABLH) Using Aerosol Lidar Data, Remote Sensing, 11, e, 2019.

Dillon, M. B., Lamanna, M. S., Schade, G. W., Goldstein, A. H., and Cohen, R. C.: Chemical evolution of the Sacramento urban plume: Transport and oxidation, Journal of Geophysical Research: Atmospheres, 107, ACH 3-1-ACH 3-15, https://doi.org/10.1029/2001JD000969, 2002.

530

Dupont, J. C., Haeffelin, M., Badosa, J., Elias, T., Favez, O., Petit, J. E., Meleux, F., Sciare, J., Crenn, V., and Bonne, J. L.: Role of the boundary layer dynamics effects on an extreme air pollution event in Paris, Atmospheric Environment, 141, 571-579, https://doi.org/10.1016/j.atmosenv.2016.06.061, 2016.

535   Elbern, H., Strunk, A., Schmidt, H., and Talagrand, O.: Emission rate and chemical state estimation by 4-dimensional variational inversion, Atmos. Chem. Phys., 7, 3749-3769, https://doi.org/10.5194/acp-7-3749-2007, 2007.

540   Fraunhofer-Institut für Solare Energiesysteme ISE: Energy-Charts, [online] Available at https://www.energy-charts.info/charts/power/chart.htm?l=de&c=DE&year=2020&source=fossil_brown_coal_lignite_unit&stacking=stacked_absolute_area&legendItems=00000000000000000000000011110&interval=week&week=19 and https://www.energy-charts.info/charts/power/chart.htm?l=de&c=DE&year=2020&source=fossil_brown_coal_lignite_unit&stacking=stacked_absolute_area&legendItems=00000000000000000000000011110&interval=week&week=-2

545   (Accessed 14 October 2021), 2021 Energy-Charts, https://energy-charts.info/index.html?l=en&c=DE

    Flynn, C. M., Pickering, K. E., Crawford, J. H., Lamsal, L., Krotkov, N., Herman, J., Weinheimer, A., Chen, G., Liu, X., Szykman, J., Tsay, S.-C., Loughner, C., Hains, J., Lee, P., Dickerson, R. R., Stehr, J. W., and Brent, L.: Relationship between column-density and surface mixing ratio: Statistical analysis of O3 and NO2 data from the

550   July 2011 Maryland DISCOVER-AQ mission, Atmospheric Environment, 92, 429-441, https://doi.org/10.1016/j.atmosenv.2014.04.041, 2014.

    Flynn, C. M., Pickering, K. E., Crawford, J. H., Weinheimer, A. J., Diskin, G., Thornhill, K. L., Loughner, C., Lee, P., and Strode, S. A.: Variability of O3 and NO2 profile shapes during DISCOVER-AQ: Implications for satellite observations and comparisons to model-simulated profiles, Atmospheric Environment, 147, 133-156,

555   https://doi.org/10.1016/j.atmosenv.2016.09.068, 2016.

    Gkatzelis, G. I., Gilman, J. B., Brown, S. S., Eskes, H., Gomes, A. R., Lange, A. C., McDonald, B. C., Peischl, J., Petzold, A., Thompson, C. R., and Kiendler-Scharr, A.: The global impacts of COVID-19 lockdowns on

560   urban air pollution: A critical review and recommendations, Elementa: Science of the Anthropocene, 9, https://doi.org/10.1525/elementa.2021.00176, 2021a.

    Gkatzelis, G. I., Coggon, M. M., McDonald, B. C., Peischl, J., Aikin, K. C., Gilman, J. B., Trainer, M., and Warneke, C.: Identifying Volatile Chemical Product Tracer Compounds in U.S. Cities, Environmental Science

565   & Technology, 55, 188-199, https://doi.org/10.1021/acs.est.0c05467, 2021b.

    He, J., Gong, S., Yu, Y., Yu, L., Wu, L., Mao, H., Song, C., Zhao, S., Liu, H., Li, X., and Li, R.: Air pollution characteristics and their relation to meteorological conditions during 2014–2015 in major Chinese cities, Environmental Pollution, 223, 484-496, https://doi.org/10.1016/j.envpol.2017.01.050, 2017.

570

    Henschel, S., Querol, X., Atkinson, R., Pandolfi, M., Zeka, A., Le Tertre, A., Analitis, A., Katsouyanni, K., Chanel, O., Pascal, M., Bouland, C., Haluza, D., Medina, S., and Goodman, P. G.: Ambient air SO2 patterns in 6 European cities, Atmospheric Environment, 79, 236-247, https://doi.org/10.1016/j.atmosenv.2013.06.008, 2013.

575

    Horel, J., Crosman, E., Jacques, A., Blaylock, B., Arens, S., Long, A., Sohl, J., and Martin, R.: Summer ozone concentrations in the vicinity of the Great Salt Lake, Atmospheric Science Letters, 17, 480-486, https://doi.org/10.1002/asl.680, 2016.

580   Hundt, P. M., Tuzson, B., Aseev, O., Liu, C., Scheidegger, P., Looser, H., Kapsalidis, F., Shahmohammadi, M., Faist, J., and Emmenegger, L.: Multi-species trace gas sensing with dual-wavelength QCLs, Applied Physics B, 124, 108, 10.1007/s00340-018-6977-y, 2018.

    Jülich Supercomputing Centre. JURECA: Modular supercomputer at Jülich Supercomputing Centre. Journal of

585   large-scale research facilities, 4, A132. http://dx.doi.org/10.17815/jlsrf-4-121-1, 2018.

    Jury, M. R.: Meteorology of air pollution in Los Angeles, Atmospheric Pollution Research, 11, 1226-1237, https://doi.org/10.1016/j.apr.2020.04.016, 2020.

590   Kuenen, J. J. P., Visschedijk, A. J. H., Jozwicka, M., and Denier van der Gon, H. A. C.: TNO-MACC_II emission inventory; a multi-year (2003-2009) consistent high-resolution European emission inventory for air quality modelling, Atmos. Chem. Phys., 14, 10963-10976, https://doi.org/10.5194/acp-14-10963-2014, 2014.

595   Lampilahti, J., Manninen, H. E., Nieminen, T., Mirme, S., Ehn, M., Pullinen, I., Leino, K., Schobesberger, S., Kangasluoma, J., Kontkanen, J., Järvinen, E., Väänänen, R., Yli-Juuti, T., Krejci, R., Lehtipalo, K., Levula, J., Mirme, A., Decesari, S., Tillmann, R., Worsnop, D. R., Rohrer, F., Kiendler-Scharr, A., Petäjä, T., Kerminen, V. M., Mentel, T. F., and Kulmala, M.: Zeppelin-led study on the onset of new particle formation in the planetary boundary layer, Atmos. Chem. Phys. Discuss., 2021, 1-32, https://doi.org/10.5194/acp-2021-282, 600   2021.

Lelieveld, J., Evans, J. S., Fnais, M., Giannadaki, D., and Pozzer, A.: The contribution of outdoor air pollution sources to premature mortality on a global scale, Nature, 525, 367-371, https://doi.org/10.1038/nature15371, 2015.

605

Li, J., Wang, Y., Zhang, R., Smeltzer, C., Weinheimer, A., Herman, J., Boersma, K. F., Celarier, E. A., Long, R. W., Szykman, J. J., Delgado, R., Thompson, A. M., Knepp, T. N., Lamsal, L. N., Janz, S. J., Kowalewski, M. G., Liu, X., and Nowlan, C. R.: Comprehensive evaluations of diurnal NO2 measurements during DISCOVER-AQ 2011: effects of resolution-dependent representation of NOx emissions, Atmos. Chem. Phys., 21, 11133-610   11160, 10.5194/acp-21-11133-2021, 2021.

Li, R., Wang, Z., Cui, L., Fu, H., Zhang, L., Kong, L., Chen, W., and Chen, J.: Air pollution characteristics in China during 2015–2016: Spatiotemporal variations and key meteorological factors, Science of The Total Environment, 648, 902-915, https://doi.org/10.1016/j.scitotenv.2018.08.181, 2019.

615

Li, X., Rohrer, F., Hofzumahaus, A., Brauers, T., Haseler, R., Bohn, B., Broch, S., Fuchs, H., Gomm, S., Holland, F., Jager, J., Kaiser, J., Keutsch, F. N., Lohse, I., Lu, K. D., Tillmann, R., Wegener, R., Wolfe, G. M., Mentel, T. F., Kiendler-Scharr, A., and Wahner, A.: Missing Gas-Phase Source of HONO Inferred from Zeppelin Measurements in the Troposphere, Science, 344, 292-296, https://doi.org/10.1126/science.1248999, 620   2014.

Lin, J.-T., and McElroy, M. B.: Impacts of boundary layer mixing on pollutant vertical profiles in the lower troposphere: Implications to satellite remote sensing, Atmospheric Environment, 44, 1726-1739, https://doi.org/10.1016/j.atmosenv.2010.02.009, 2010.

625

Liu, C.; Tuzson, B.; Scheidegger, P.; Looser, H.; Bereiter, B.; Graf, M.; Hundt, M.; Aseev, O.; Maas, D.; Emmenegger, L. Laser driving and data processing concept for mobile trace gas sensing: design and implementation. Rev. Sci. Instrum. 89 (6), 065107 (9 pp.). https://doi.org/10.1063/1.5026546, 2018

630   Liu, F., Beirle, S., Zhang, Q., Dörner, S., He, K., and Wagner, T.: NOx lifetimes and emissions of cities and power plants in polluted background estimated by satellite observations, Atmos. Chem. Phys., 16, 5283-5298, https://doi.org/10.5194/acp-16-5283-2016, 2016.

Marenco, A., Thouret, V., Nédélec, P., Smit, H., Helten, M., Kley, D., Karcher, F., Simon, P., Law, K., Pyle, J., 635   Poschmann, G., Wrede, R. V., and Cook, C. H. T.: Measurement of ozone and water vapor by Airbus in-service aircraft: The MOZAIC airborne program, an overview, Journal of Geophysical Research: Atmospheres, 103, 25631-25642, https://doi.org/10.1029/98JD00977, 1998.

Molina, L. T., Madronich, S., Gaffney, J. S., Apel, E., de Foy, B., Fast, J., Ferrare, R., Herndon, S., Jimenez, J. 640   L., Lamb, B., Osornio-Vargas, A. R., Russell, P., Schauer, J. J., Stevens, P. S., Volkamer, R., and Zavala, M.: An overview of the MILAGRO 2006 Campaign: Mexico City emissions and their transport and transformation, Atmos. Chem. Phys., 10, 8697-8760, https://doi.org/10.5194/acp-10-8697-2010, 2010.

Nieminen, T., Yli-Juuti, T., Manninen, H. E., Petäjä, T., Kerminen, V. M., and Kulmala, M.: Technical note: 645   New particle formation event forecasts during PEGASOS–Zeppelin Northern mission 2013 in Hyytiälä, Finland, Atmos. Chem. Phys., 15, 12385-12396, https://doi.org/10.5194/acp-15-12385-2015, 2015.

Ouchi, M., Matsumi, Y., Nakayama, T., Shimizu, K., Sawada, T., Machida, T., Matsueda, H., Sawa, Y., Morino, I., Uchino, O., Tanaka, T., and Imasu, R.: Development of a balloon-borne instrument for CO2 vertical profile 650   observations in the troposphere, Atmos. Meas. Tech., 12, 5639-5653, https://doi.org/10.5194/amt-12-5639-2019, 2019.

Pernigotti, D., Georgieva, E., Thunis, P., and Bessagnet, B.: Impact of meteorology on air quality modeling over the Po valley in northern Italy, Atmospheric Environment, 51, 303-310, https://doi.org/10.1016/j.atmosenv.2011.12.059, 2012.

Petzold, A., Thouret, V., Gerbig, C., Zahn, A., Brenninkmeijer, C. A. M., Gallagher, M., Hermann, M., Pontaud, M., Ziereis, H., Boulanger, D., Marshall, J., Nedelec, P., Smit, H. G. J., Friess, U., Flaud, J. M., Wahner, A., Cammas, J. P., Volz-Thomas, A., and Team, I.: Global-scale atmosphere monitoring by in-service aircraft - current achievements and future prospects of the European Research Infrastructure IAGOS, Tellus Series B-Chemical and Physical Meteorology, 67, https://doi.org/10.3402/tellusb.v67.28452, 2015.

Powers, J. G., Klemp, J. B., Skamarock, W. C., Davis, C. A., Dudhia, J., Gill, D. O., Coen, J. L., Gochis, D. J., Ahmadov, R., Peckham, S. E., Grell, G. A., Michalakes, J., Trahan, S., Benjamin, S. G., Alexander, C. R., Dimego, G. J., Wang, W., Schwartz, C. S., Romine, G. S., Liu, Z., Snyder, C., Chen, F., Barlage, M. J., Yu, W., and Duda, M. G.: The Weather Research and Forecasting Model: Overview, System Efforts, and Future Directions, Bulletin of the American Meteorological Society, 98(8), 1717-1737, https://doi.org/10.1175/BAMS-D-15-00308.1, 2017.

Pöschl, U., von Kuhlmann, R., Poisson, N., and Crutzen, P. J.: Development and Intercomparison of Condensed Isoprene Oxidation Mechanisms for Global Atmospheric Modeling, Journal of Atmospheric Chemistry, 37, 29-52, https://doi.org/10.1023/A:1006391009798, 2000.

Ramonet, M., Wagner, A., Schulz, M., Errera, Q., Eskes, H. J., Basart, S., Benedictow, A., Bennouna, Y., Blechschmidt, A.-M., S. Chabrillat, C., Y., E. C., El-Yazidi, A., Flentje, H., Fritzsche, P., Hansen, K. M., Im, U., Kapsomenakis, J., Langerock, B., Richter, A., Sudarchikova, N., Thouret, V., Warneke, T., and Zerefos, C.: Validation report of the CAMS near-real-time global atmospheric composition service, https://doi.org/10.24381/8pxnq362, 2020.

Romer, P. S., Duffey, K. C., Wooldridge, P. J., Allen, H. M., Ayres, B. R., Brown, S. S., Brune, W. H., Crounse, J. D., de Gouw, J., Draper, D. C., Feiner, P. A., Fry, J. L., Goldstein, A. H., Koss, A., Misztal, P. K., Nguyen, T. B., Olson, K., Teng, A. P., Wennberg, P. O., Wild, R. J., Zhang, L., and Cohen, R. C.: The lifetime of nitrogen oxides in an isoprene-dominated forest, Atmos. Chem. Phys., 16, 7623-7637, https://doi.org/10.5194/acp-16-7623-2016, 2016.

Ryerson, T. B., Buhr, M. P., Frost, G. J., Goldan, P. D., Holloway, J. S., Hübler, G., Jobson, B. T., Kuster, W. C., McKeen, S. A., Parrish, D. D., Roberts, J. M., Sueper, D. T., Trainer, M., Williams, J., and Fehsenfeld, F. C.: Emissions lifetimes and ozone formation in power plant plumes, Journal of Geophysical Research: Atmospheres, 103, 22569-22583, https://doi.org/10.1029/98JD01620, 1998.

Ryerson, T. B., Andrews, A. E., Angevine, W. M., Bates, T. S., Brock, C. A., Cairns, B., Cohen, R. C., Cooper, O. R., de Gouw, J. A., Fehsenfeld, F. C., Ferrare, R. A., Fischer, M. L., Flagan, R. C., Goldstein, A. H., Hair, J. W., Hardesty, R. M., Hostetler, C. A., Jimenez, J. L., Langford, A. O., McCauley, E., McKeen, S. A., Molina, L. T., Nenes, A., Oltmans, S. J., Parrish, D. D., Pederson, J. R., Pierce, R. B., Prather, K., Quinn, P. K., Seinfeld, J. H., Senff, C. J., Sorooshian, A., Stutz, J., Surratt, J. D., Trainer, M., Volkamer, R., Williams, E. J., and Wofsy, S. C.: The 2010 California Research at the Nexus of Air Quality and Climate Change (CalNex) field study, Journal of Geophysical Research: Atmospheres, 118, 5830-5866, https://doi.org/10.1002/jgrd.50331, 2013.

Seinfeld, J. a. P., S.: Atmospheric Chemistry And Physics: From Air Pollution to Climate Change, second edition ed., Wiley-Interscience Publication, Hoboken, NJ, USA, 2006.

Silcox, G. D., Kelly, K. E., Crosman, E. T., Whiteman, C. D., and Allen, B. L.: Wintertime PM2.5 concentrations during persistent, multi-day cold-air pools in a mountain valley, Atmospheric Environment, 46, 17-24, https://doi.org/10.1016/j.atmosenv.2011.10.041, 2012.

Skamarock, W. C., Klemp, J. B., Dudhia, J., Gill, D. O., Barker, D., Duda, M. G., Huang X.,Wang, W., Powers, J. G. A Description of the Advanced Research WRF Version 3 (No. NCAR/TN-475+STR). University Corporation for Atmospheric Research. https://doi.org/10.5065/D68S4MVH, 2008

Stull, R. B.: An Introduction to Boundary Layer Meteorology, Kluwer Academic Publishers, Dordrecht, Boston and London, 666 pp., http://dx.doi.org/10.1007/978-94-009-3027-8, 1988.

Umweltbundesamt: Aktuelle Luftdaten, [online] Available from:
https://www.umweltbundesamt.de/daten/luft/luftdaten/stationen (Accessed 14 October 2021), 2021

715

Valin, L. C., Russell, A. R., and Cohen, R. C.: Variations of OH radical in an urban plume inferred from NO2
column measurements, Geophysical Research Letters, 40, 1856-1860, https://doi.org/10.1002/grl.50267, 2013.

720 Veefkind, J. P., Aben, I., McMullan, K., Förster, H., de Vries, J., Otter, G., Claas, J., Eskes, H. J., de Haan, J. F.,
Kleipool, Q., van Weele, M., Hasekamp, O., Hoogeveen, R., Landgraf, J., Snel, R., Tol, P., Ingmann, P., Voors,
R., Kruizinga, B., Vink, R., Visser, H., and Levelt, P. F.: TROPOMI on the ESA Sentinel-5 Precursor: A GMES
mission for global observations of the atmospheric composition for climate, air quality, time periods and ozone
layer applications, Remote Sensing of Environment, 120, 70-83, https://doi.org/10.1016/j.rse.2011.09.027, 2012.

725 Villa, T. F., Gonzalez, F., Miljievic, B., Ristovski, Z. D., and Morawska, L.: An Overview of Small Unmanned
Aerial Vehicles for Air Quality Measurements: Present Applications and Future Prospectives, Sensors, 16, 1072,
https://doi.org/10.3390/s16071072, 2016.

Werle, P., Mücke, R., and Slemr, F.: The limits of signal averaging in atmospheric trace-gas monitoring by
730 tunable diode-laser absorption spectroscopy (TDLAS), Applied Physics B, 57, 131-139,
https://doi.org/10.1007/BF00425997, 1993.

Zhao, S., Yu, Y., Qin, D., Yin, D., Dong, L., and He, J.: Analyses of regional pollution and transportation of
$PM_{2.5}$ and ozone in the city clusters of Sichuan Basin, China, Atmospheric Pollution Research, 10, 374-385,
735 https://doi.org/10.1016/j.apr.2018.08.014, 2019.

Zhao, Z., Chen, S.-H., Kleeman, M. J., and Mahmud, A.: The Impact of Climate Change on Air Quality–Related
Meteorological Conditions in California. Part II: Present versus Future Time Simulation Analysis, Journal of
Climate, 24, 3362-3376, https://doi.org/10.1175/2010JCLI3850.1, 2011.

740